Construction and Building Materials 256 (2020) 119471

Contents lists available at ScienceDirect

Construction and Building Materials

journal homepage: www.elsevier.com/locate/conbuildmat

Penetration of water into cracked geopolymer mortars by means of neutron radiography

A. El Abd [a], S.E. Kichanov [b], M. Taman [c,*], K.M. Nazarov [b,d]

[a] Reactor Physics Department, Nuclear Research Center, Egyptian Atomic Energy Authority, 13759 Abu Zaabal, Egypt
[b] Frank Laboratory of Neutron Physics, Joint Institute for Nuclear Research, 141980 Dubna, Russia
[c] Department of Structural Engineering, Faculty of Engineering, Tanta University, 31511 Tanta, Egypt
[d] Gumilev Eurasian National University, Nur-Sultan 010008, Kazakhstan

HIGHLIGHTS

- Geopolymer is an eco-friendly innovative construction material.
- For the first time, water absorption into cracked geopolymer mortars was introduced.
- The external waterproofing slurry reduced water ingress more than the internal one.
- Water invaded the externally protected sample from the crack region.
- The water absorption processes followed the square root of absorption time.

ARTICLE INFO

Article history:
Received 11 November 2019
Received in revised form 2 May 2020
Accepted 5 May 2020
Available online 8 May 2020

Keywords:
Geopolymer mortar
Neutron radiography
Water ingress
Moisture absorption
Waterproofing additives
Profiles

ABSTRACT

Water transport into cracked fly ash geopolymer mortars were investigated, for the first time, using neutron radiography. Three samples were prepared and cracks were induced in these samples. The first sample does not contain internal waterproofing additives, the second contains Lignosulphonates based waterproofing admixture and the third sample was covered with external waterproofing slurry coat. Neutron radiography images were acquired continuously during the moisture absorption process. The results obtained showed that water absorption into first sample is the fastest. The internal waterproofing additives minimized water absorption into the second sample. The waterproofing slurry coat stopped water ingress into the third sample for 109 min, however after that time it started to absorb water from the crack region only. Water is fed to all portions of the samples from the water filled cracks. The advance of water from the cracks into the matrix of the samples follows the square root of the absorption time.

1. Introduction

Portland cement (PC) is considered the backbone of the construction industry all over the world. It is estimated that the manufacturing of one tone of cement emits 0.8 tonnes of CO_2 per ton of Portland cement [1,2,3]. The cement industry is considered the second largest producer of CO_2 (5–8% of worldwide emissions) [1,2,3]. In addition to its aggressive environmental impact, it leads to the consumption of the natural resources of raw materials [4]. Thus, it is necessary to find alternatives to produce an eco-friendly concrete [5]. The using of supplementary cementitious materials (silica fume, fly ash, GGBFS,...etc.) as a replacement of PC is one of these alternatives. For instance, incorporating up to 60% of fly ash as a replacement of PC achieved high mechanical properties and improved the durability performance [6]. Concretes characterized with high compressive strength and fracture toughness can be produced by replacing cement by fly ash [3]. Additionally, the properties of the concretes containing fly ash depend on the age of the concrete [3,7]. It was reported that as the percentage of fly ash in concrete increases, the drying shrinkage decreases [7–9]. Lower water sorptivity, permeability, and chloride permeability were reported for fly ash concrete [7]. GGBFS are used in the mixture of high-performance concrete (HPC) as a kind of mineral admixture [10–14]. It was reported that the properties of concrete, such as durability, workability and long-term strength can be improved by addition of GGBFS [10]. As the GGBFS content increases, the autogenous shrinkage increases [11], cracking potential of HPC decreases [12,14], and the total shrinkage, porosity, and mobility of chloride ions decrease [13,14]. It was shown that

* Corresponding author.
E-mail address: mohamed.taman@f-eng.tanta.edu.eg (M. Taman).

https://doi.org/10.1016/j.conbuildmat.2020.119471
0950-0618/

alkali-activated slag/fly ash-based pastes are more resistant to phosphoric acid attacks compared to ordinary PC-based pastes [15]. Sulfate resistance of PC-slag concrete generally decreased with increasing slag content [16,17]. It was reported that sorptivity and resistance to sulphate, acid and chloride attacks improve with increase in the content of GGBFS replacing PC in recycled aggregate concrete (RAC) [17]. Geopolymer is a new form of binder free from cement and produced by the reaction of aluminosilicate material with alkaline solutions. In early 1980 s, geopolymer was firstly introduced as an eco-friendly artificial stone with excellent mechanical properties [18,19]. Slag, fly ash (a by-product obtained in the process of hard coal combustion) and metakaolin were used as sources to the silica and alumina in the geopolymer matrix. Low calcium fly ash is the common pozzolanic material used in geopolymer manufacturing. The alkaline activator almost consists of sodium silicate (Na_2SiO_3) and sodium hydroxide (NaOH) [20,21]. The final properties of produced geopolymer concrete and/or mortar depend on the mixing ratio of these components. On the other hand, a heat curing is preferable to accelerate the reaction [22]. In addition to its highly mechanical properties, a significant low chloride penetration was recorded compared to that of cementitious concrete [23]. It leads to be recommended as a protection or repair material.

Water penetration into porous media including construction building materials is so important physical process. It is the cause for many damage mechanisms [24]. For brick, due to the long direct contact of a brick wall with the ground, ground water carrying soluble salts and harmful chemical substances penetrates into the wall components by capillary forces leading to dampening and salting them [24]. This may contribute to the so-called moisture destruction [24,25] which increases over time. Water-soluble salts cause crystallization and hydration processes near and on the surface of the wall leading to breaking up the masonry structure and forming surface salt efflorescence [24]. Pressure in the pores and capillaries of the structure increases as a result of crystallization and hydration processes that occur continuously. The structure breaks after the pressure in the pores and capillaries of the structure exceeds a threshold limit [24]. In the presence of water (either from ground water or rains or both), biodeterioration [26,27] is accelerated by the growth of micro-organisms and hydrolysis of the binding matrix of cement-based materials. Since absorbed water may carry dissolved harmful chemicals, acids are formed inside the pore space. This leads to the so-called acid attack. Also, sulfate attack, chloride attack and carbonation may occur. Reinforcement steel corrosion may be a consequence of both chloride attack and carbonation. Moreover, water saturated porous materials are not frost resistant. Drying of a wetted porous medium [27–29] causes shrinkage, which usually causes formation of cracks [30,31]. Additionally, due to the freeze/thaw cycles [32–34], width of cracks could be increased. These cracks interconnect flow paths for water that may contain dissolved and harmful chemicals. The width of crack is critical, where only the capillary cracks can help in water capillarity. This leads to further increasing the rate of steel corrosion. Certainly, the service life and durability of many construction building materials including cement-based materials are shortened in short time [35–37]. Several methods are used to minimize moisture transport in either cracked or uncracked samples of porous building materials such as surface treatment [38], internal curing, and self-healing [39]. Further details can be found in Zhang et al., [27].

Research on durability of geopolymers including decreasing sorptivities and/or capillary absorption coefficients are based on microstructure densification and pore refinement due to adjusting of curing conditions and mix proportions or the addition of mineral admixtures [40]. Geopolymers based mortars and/or concrete characterized with lower sorptivities were reported as presented by Zhang et al., [40]. The reported improvement in many durability issues were based on the internal modification of the geopolymer matrix. However, few works on modification of the surface of the geopolymer were reported. Duan et al. [41] and Xue et al., [42] proposed surface waterproof agents for geopolymer based on alkali activation of metakaolin and for low-calcium fly ash pastes, respectively. The addition of surface hydrophobic modifier results in a remarkable reduction in water absorption [41,42]. Commercially available agents to seal cracks were used to reduce water absorption effectively [43,44]. A polyurethane based and water repellent agents are examples for these agents. Both agents were used effectively to seal cracks for cement-based materials. Cracks containing encapsulated healing agent can be autonomously healed.

Neutron radiography (NR) is a powerful non-destructive imaging technique [45,46]. It is based on the transmission of a neutron beam by the sample under investigation according to the Beer-Lambert law. The transmitted beam is registered by using a suitable recording system such as a charge coupled device (CCD) camera. A 2-dimentional image is produced carrying important information about the sample under investigation. Due to the large incoherent cross section of hydrogen, contained in water for thermal neutrons in comparisons with matrix of a porous medium, it is possible to apply NR to study transport of liquids in construction building materials. Generally, there is a jump in the different applications of NR because the availabilities of high neutron fluxes and the use of digital imaging based on CCD cameras [27,47]. Nowadays, NR experiments with excellent spatial resolutions are carried out to investigate fast as well as slow dynamical processes [27,47–55] such as water and/or moisture transport in porous media including construction building materials (bricks, mortars, concrete,... etc.). The different applications of neutron radiography to investigate moisture transport in porous media including construction building materials under various conditions have been extensively discussed [27,47].

NR was successfully used to study water absorption into cement-based materials. These studies included water absorption into cracked and uncracked cement-based mortars and/or concrete samples and the use of the different agents to minimize water ingress including hydrophobic treatment methods [30,31,44,56–62]. However, NR was not used to investigate water absorption into cracked geopolymer mortars and/or concretes. Also, studies related to the effect of the hydrophobic treatment methods on water absorption of cracked geopolymer mortars and /or concretes are rare.

Therefore, in this work we use NR to investigate moisture transport in cracked geopolymer mortars, for the first time. The cracked samples were treated from the surface and internally cured with a commercially available hydrophobic material.

2. Samples preparation and experimental details

Geopolymer mortar was the main matrix for preparing the investigated samples and consists as follows; **fly ash class F**, low-calcium (this classification is according to the chemical composition of ASTM C618-19 where low CaO is less than 3%), with specific surface area of about 480 m^2/kg and specific weight of 2.24 was used; **alkaline solution** consists of sodium hydroxide NaOH and sodium silicate Na_2SiO_3 (SiO_2 = 29.4%, Na_2O = 14.7% and water = 55.9%) was utilized as activator. NaOH with 98% purity and in pellets form used for 16 M solution. The two solutions (sodium hydroxide and sodium silicate) were mixed to form the alkaline solution; **river siliceous sand** free from impurities (this was performed according to the standard test ASTM C87-C87M-17), fineness modulus of 2.36 (this was determined through sieve analysis test ASTM C136-C136M-179) and its water absorption less

than 0.8% (water absorption was determined after 24 hrs of water soaking for a dry sand sample), represents the fine aggregate; **tab water** (pH value of = 7.2 and total dissolved salts = 0.14 gm/Liter) was used as an extra water to enhance the consistency (make it more flowable) of the mortar; **Lignosulphonates** based waterproofing admixture was used as an internal waterproofing admixture of dosage about 1% by mass of the fly ash. It was used in the mixing of geopolymer mortar Mix#2 as additional investigated parameter. Mix#1 is geopolymer mortar mix without internal waterproofing additives. Table 1 lists mix proportions by weight for the tested geopolymer mortar mixes. All the ingredients were mixed together for 8 min then placed in prismatic molds with 300x100x100 mm as shown in Fig. 1a. The molds were left in lab temperature (25 ± 2 °C) for 24 hrs followed by heat curing in special chamber at 65 ± 2C for another 48 hrs. Fig. 1b shows the hardened geopolymer mortar after the heat curing. The compressive strength of the proposed mix achieved approximately 32 MPa after the heat curing for cube 50x50x50 mm specimens.

Each prismatic specimen (300x100x100 mm) was reinforced with 9 steel reinforcing rebars of 2 mm diameter arranged as shown in Fig. 1c. After the heat curing each prism was cut into three identical slices (300x100x30 mm) with a diamond saw along the long axis of the prisms as shown in Fig. 1c. Each slice was tested under three-point loading, flexure test, in order to crack induce. To perform the test, a universal testing machine with data acquisition system was used and the crack width was recorded using Linear Variable Differential Transformer (LVDT) as shown in Fig. 1d. For all investigated samples crack width of 0.4 ± 0.05 m m was achieved. After crack creation the slice unloaded and the middle 100 mm (containing the crack at the center) was cut. The slices were dried in a ventilated oven at 110 °C for 2 days, where constant weight was achieved.

External polymeric waterproofing slurry, which is used to protect the concrete structures through the reduction of water ingress and chloride penetration ions, was used to cover the external surface of the sample. Two perpendicular layers of the waterproofing slurry coat (with total thickness not less than 2 mm) were applied after the specimens were wetted using clean water by stiff brush. This sample is denoted Mix#3.

NR experiments of water absorption into the prepared geopolymer mortar samples were carried using the NR and tomography station placed on beamline 14 of the IBR-2 high-flux pulsed reactor, Joint Institute of Nuclear Research (JINR), Dubna, Russia [63,64]. Four of the surfaces of the Mix#1 and Mix#2 samples were covered by aluminum self-adhesive foils with the exception of the two opposite surfaces with dimension of 10x3cm. A water container with supports at the bottom was prepared. The geopolymer mortar samples Mix#1, Mix#2 and Mix#3 were fixed vertically on the supports and their ends were immersed into the water container to allow water to flow up by capillarity against gravity forces. The thickness of the samples in the direction of neutron travel was 3 cm. The level of water in the container covers ~ 3 mm of the immersed sample ends and was kept constant during the test. While the samples absorb water, NR images were registered regularly. NR images were registered by a CCD-based detector system (a maximum field of view of 20 × 20 cm). The imaging data were corrected by subtracting the camera dark current image and then, normalizing to the image of the incident neutron beam using the ImageJ software [65]. Two NR experiments were performed. The first one was carried out for Mix#1 and Mix# 2 samples and the second one for Mix#3 sample. The NR images were collected with a duration of 20 s per frame and a delay between frames of 45 sec. 331 and 470 images were collected for the first and second experiments with total exposure times of 4.1 h and 5.9 h, respectively.

Fig. 1a. Placing of specimens.

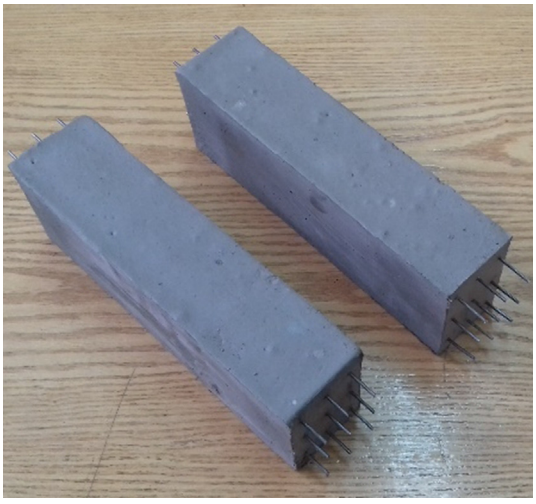

Fig. 1b. Hardened specimens.

3. Results and discussion

3.1. Mix#1 and Mix#2 samples

Fig. 2 shows some NR images obtained for Mix#1 and Mix#2 samples. As one can see, after absorption times 6.25 min and

Table 1
Mix proportions by weight for the tested geopolymer mortar mixes.

Mix ID	Fly ash	Fine aggregate	Na_2SiO_3	NaOH	Extra water	Internal Waterproofing admixture	External polymeric waterproofing slurry
Mix #1	1	2	0.27	0.13	0.10	0.0	No
Mix #2	1	2	0.27	0.13	0.05	0.01	No
Mix #3	1	2	0.27	0.13	0.05	0.0	yes

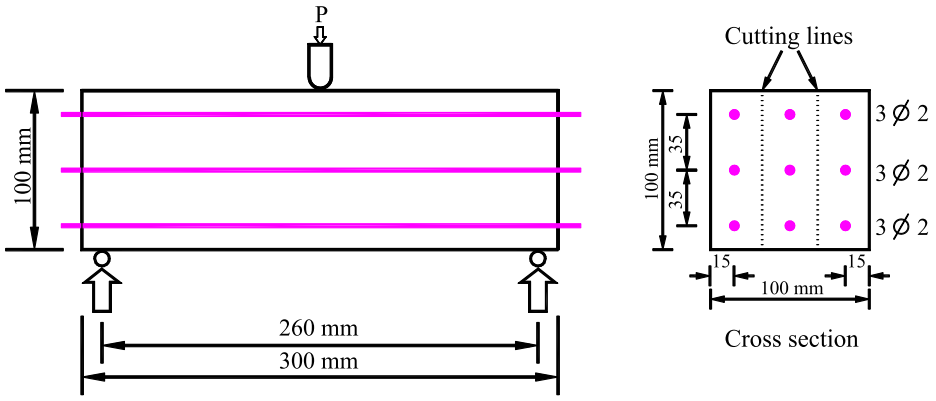

Fig. 1c. Reinforcement details, test setup and cutting lines of investigated specimens.

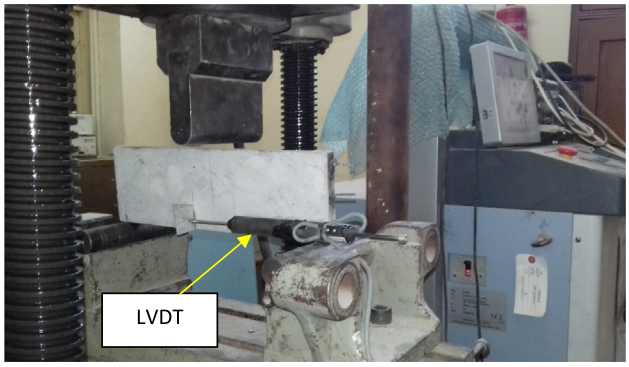

Fig. 1d. Crack creation under three-point loading.

18.25 min, the cracks of Mix#1 sample (the left sample in the NR images) and Mix#2 sample are completely filled with water, respectively. As the absorption time elapses, water spreads horizontally from the water filled cracks. Spread of water is faster for Mix#1 than Mix#2. In other words, crack of the Mix#1 drains water to matrix of the sample with higher rate than for Mix#2. This may be the reason of the delay in filling the crack of Mix#1 sample. Additionally, water absorption can be noticed from the low immersed ends in water. It is higher as well as faster for the Mix#1 than Mix#2 sample. The different behavior of water absorption is attributed to the internal waterproofing (dosage about 1% by mass of the fly ash) added to Mix#2 sample. The waterproofing agent did not prevent the water absorption, however it minimized it. On the other hand, using small dosage of LS (1% of cement content) in cement mortar reduced the total pore amount by 24.6% than the total amount without LS [66]. Additionally, pore size distribution is remarkably reduced compared with mortar samples without LS [66]. To the best knowledge of authors, the effect of lignosulphonates admixture in durability issues of geopolymer mortars and/or or concretes was not studied before [67,68]. Only, an increase in workability and a slight reduction in shrinkage, with the LS admixture of alkali-activated slag concretes were reported [69]. There is no similar data in literature to compare our results with them.

Comparisons of the water absorption behaviors and mechanisms of water flow and distribution through the cracked samples investigated were obtained by analyzing the NR images acquired. Water content distributions through the investigated samples (water profiles) were determined. Horizontal spread of water, at both sides of the cracks, was determined as the absorption time elapses at top and bottom of the samples. The profiles determined at bottom of the samples (marked by the rectangular areas number 1 and 2 shown in Fig. 2 at absorption time, T = 6.25 min) for the Mix#1 and Mix#2 are shown in Figs. 3a and 3b, respectively. Fig. 3a shows that there is no water front as the absorption time elapses, because water spreads through the sample horizontally from the crack (a second source of water) and vertically from the water container. It can be noticed that, the left and right sides of both Mix#1 and Mix#2 samples absorbed water. This is remarkably noticed for the right side for the Mix#2 sample. The absorption of water by sides of the samples is due to an improper attachment of the aluminum tape on these sides. Although the aluminum tape was always carefully applied, this problem could not always be avoided unfortunately. Such unpredicted boundary effects were observed and reported in literature [56,61,62]. The water profiles for Mix#2 sample (Fig. 3b) are more regular and smooth than for Mix#1. Water is fed to the matrix of the sample from the crack, the right side of the sample (due to the improper attachment of the aluminum tape) and from the water container. The crack feds the sample with water more than the right side of the sample. Shapes of these profiles indicate that the Mix#2 sample is more homogenous than for the Mix#1 sample. It can be noticed that, Mix#1 sample does not absorb water after an absorption time of 30 min (Fig. 3a) and until the end of the experiment since the shape of the profiles does not change, however the situation for Mix#2 sample is different. The water content increases after 30 min of absorption time. This implies that rate of absorption of water in Mix#2 sample is less than that for Mix #1 sample. Rates of water absorption can be described by the horizontal profiles at top of the samples. The side-effects due to the improper attachment of the aluminum tape are absent and do not perturb the results. These profiles were determined (marked by the rectangular areas number 3 and 4 shown in Fig. 2, at absorption time, T = 6.25 min) and are shown in Figs. 4a and 4b for the Mix#1 and Mix#2, respectively. It can be noticed that there are clear water fronts, and they are more regular for the Mix#2 sample than Mix#1. Water front positions were determined from these profiles and are shown in Fig. 5. The water front positions follow the square root of the absorption time as shown by the fit lines of least square fitting using straight line equations. The rate of water spreads can be represented by the slopes of these fit lines. It is faster for the Mix#1 than Mix#2 by a factor of 1.27.

The irregular water distributions through the Mix#1 sample can be attributed to the inhomogeneous structure of the prepared sample. Fig. 2 (at absorption time, T = 249.25 min) shows dark regions (marked by circles and ellipses). The darkness of these regions increases as the absorption time increases. These dark regions may be attributed to unreacted fly ash grains [70]. These regions are not observed in the Mix#2 sample. Absence of dark

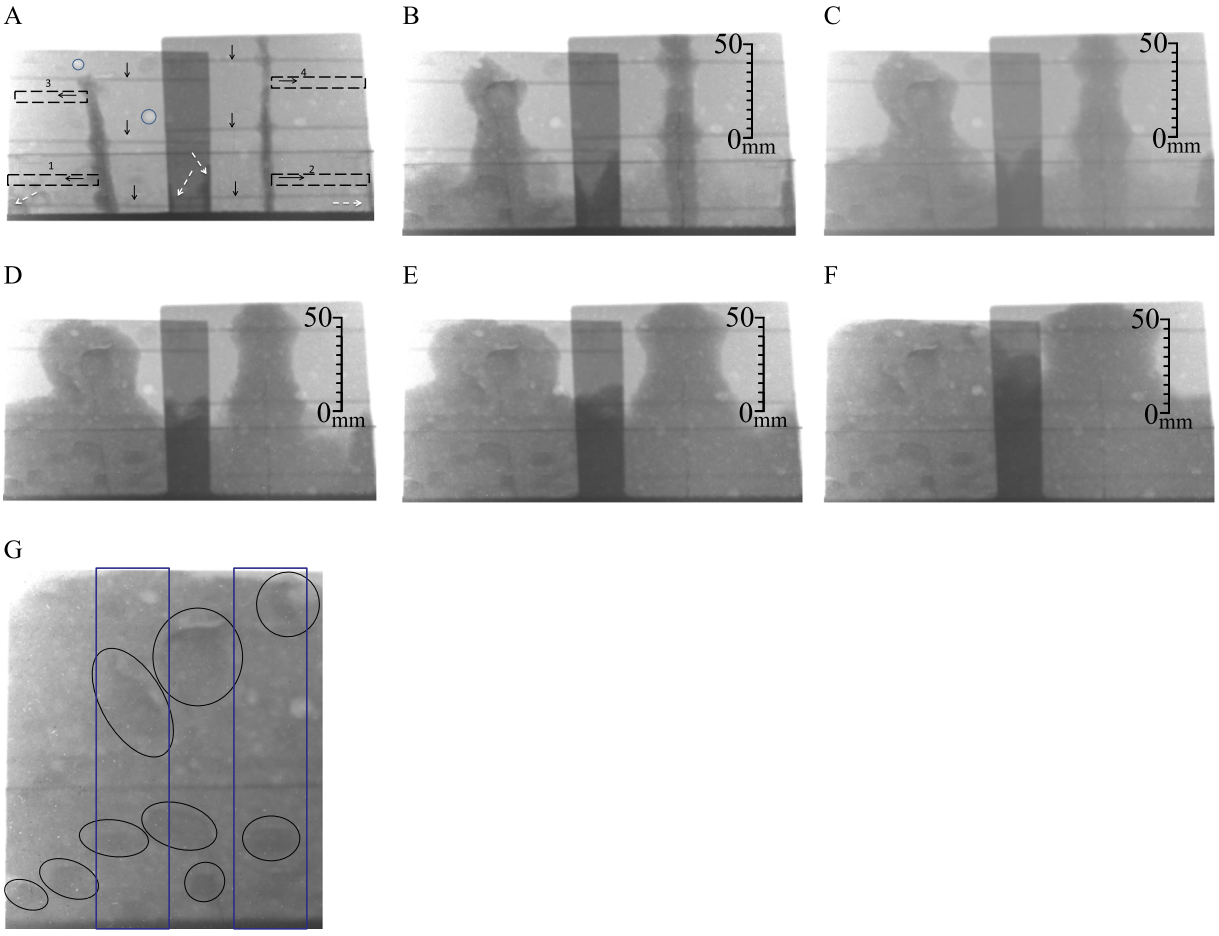

Fig. 2. NR images for Mix#1 (left) and Mix#2 (right) samples recorded at absorption times 6.25 min (A), 18.25 min (B), 40.75 min (C), 78.25 min (D), 121.75 min (E), 249.25 min (F), and 294.5 min (G). The vertical arrows refer to the steel bars, the rectangular areas mark the regions used for determining water profiles. The arrows inside the rectangles refer to directions of water flow. The circles surround some white areas of isolated voids. White arrows refer water absorption at sides of the samples due to the improper attachment of aluminum adhesive tape. The NR image acquired at the absorption time at 294.5 min (G) is a magnified image for Mix#1 sample. Circles and ellipses surround dark regions. The vertical rectangles at both sides of the crack are used for determining water profiles.

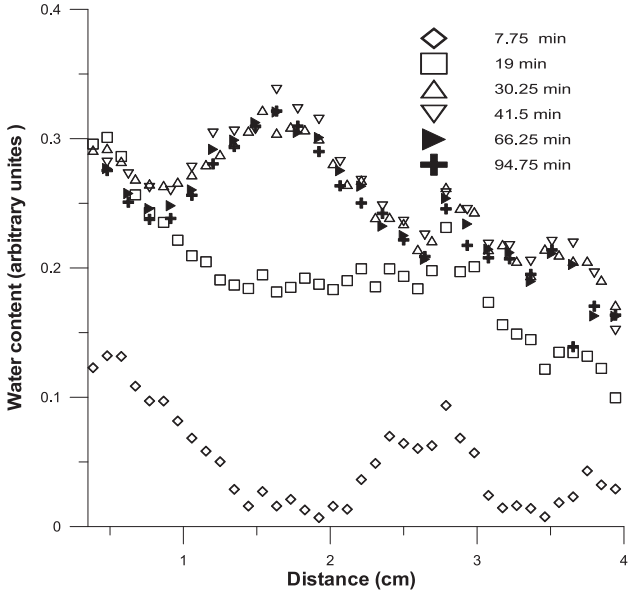

Fig. 3a. Horizontal water profiles for the left side of the crack for Mix#1 sample determined at different absorption times. Rectangle number 1 in Fig. 2 was used for determining the profiles.

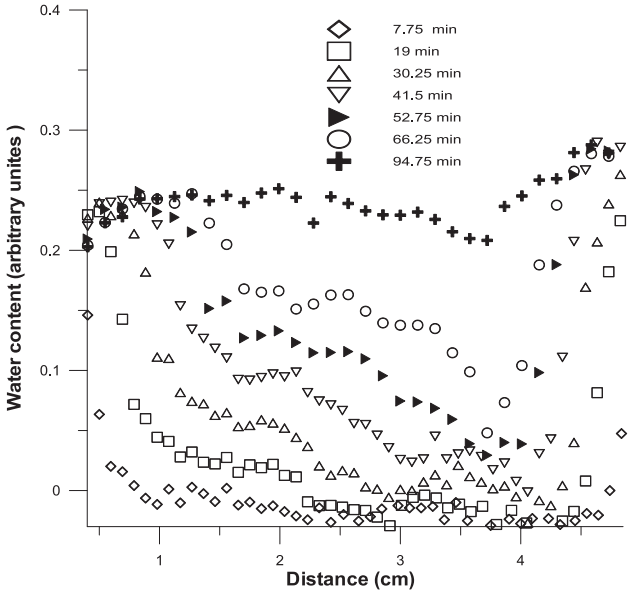

Fig. 3b. Horizontal water profiles for the right of the crack for Mix#2 sample determined at different absorption times. Rectangle number 2 in Fig. 2 was used for determining the profiles.

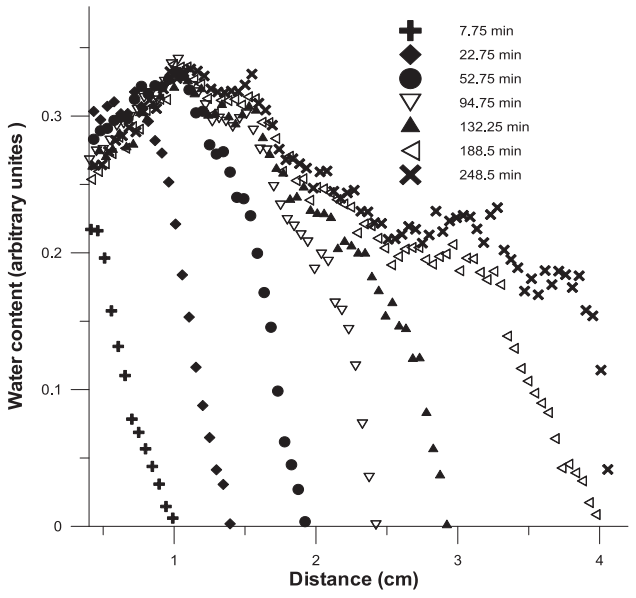

Fig. 4a. Water profiles of the left side of the crack for Mix#1 sample determined at different absorption times. Rectangle number 3 in Fig. 2, at T = 6.25 min was used for determining the profiles.

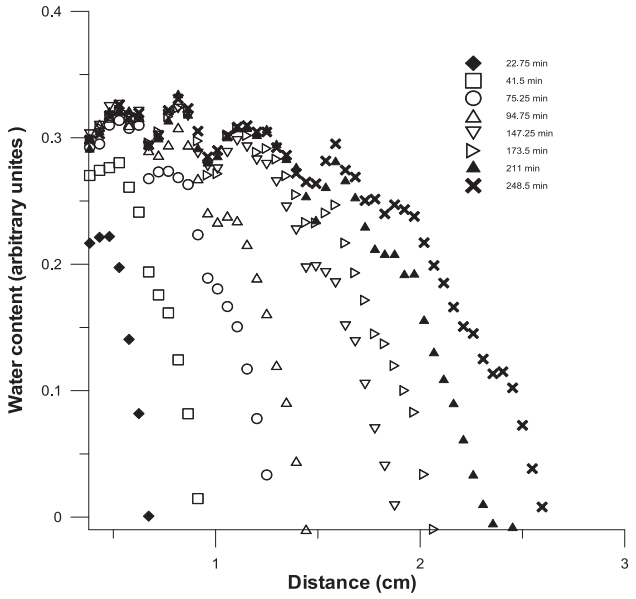

Fig. 4b. Water profiles of the right of the crack for Mix#2 sample determined at different absorption times. Rectangle number 4 in Fig. 2, at T = 6.25 min was used for determining the profiles.

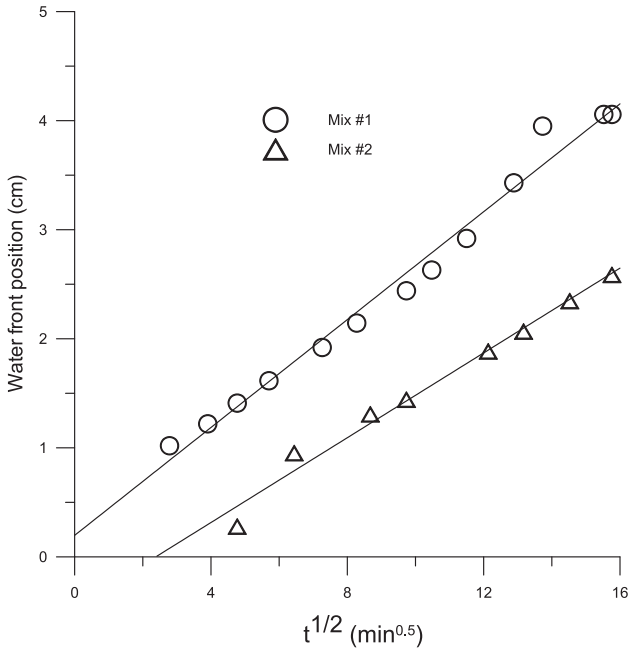

Fig. 5. Water front positions versus square root of absorption time for Mix#1 and Mix#2 samples determined from Figs. 4a and 4b at different absorption times.

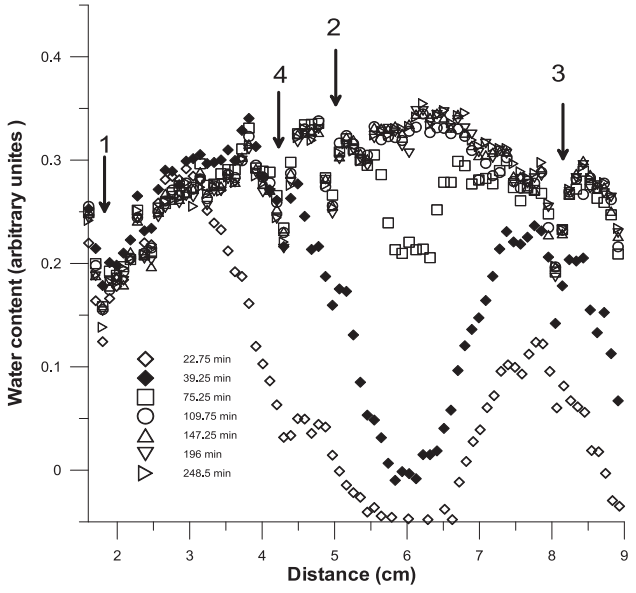

Fig. 6a. Vertical water profiles for the left side of the crack for Mix#1 sample determined at different absorption times. The left rectangle shown in Fig. 2 at absorption time, T = 249.25 min was used. Arrows number 1, 2, and 3 refer to the position of the steel bars. Arrow number 4 refers to a reference line.

regions in Mix#2 could be attributed to the LS added. Additionally, small white regions are observed in the images of the Mix#1 and Mix#2 samples (marked by circles in Fig. 2, at T = 6.25 min). These regions could be considered isolated voids, since they are not filled with water during the experiment. Namely, if these regions were filled with water, they should be darker than the surroundings.

Two vertical rectangular areas at the left and right sides of the crack, shown in Fig. 2 at absorption time, T = 249.25 min for the Mix#1 sample, were used to determine the vertical water profiles. The results are shown in Figs. 6a and 6b for the left and right sides of the crack, respectively. The profiles for the right side are different from those for the left side. The right profiles are more regular than that of the left ones which confirm that structure of this sample is not homogenous. The positions of the steel bars are clearly seen from these results. Corresponding vertical water profiles for the Mix#2 sample at the left and right sides of the crack are shown Figs. 7a and 7b, respectively. In contrast to the profiles of the Mix#1 sample, the profiles for the Mix#2 sample at both sides of the crack are similar to each other. This indicates that, Mix#2 sample is more homogenous than Mix#1 sample. The vertical profiles for both Mix#1 and Mix#2 samples indicate that the left and right sides of the cracks are fed water from both the cracks and the water container.

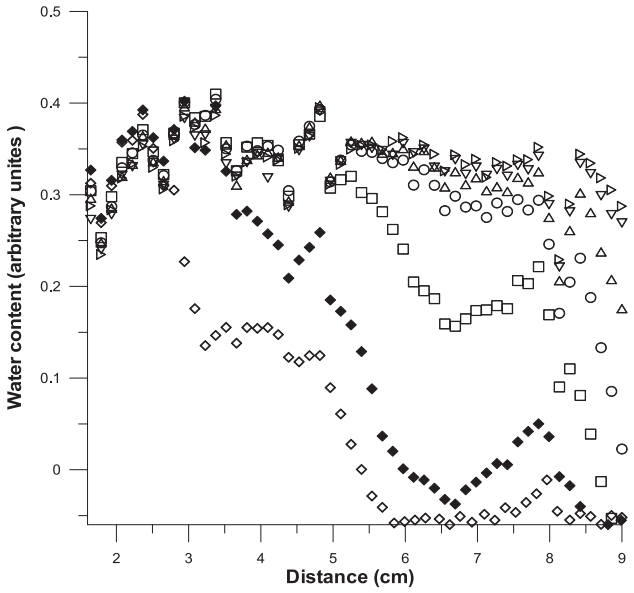

Fig. 6b. Vertical water profiles for the right side of the crack for Mix#1 sample determined at the same absorption times of Fig. 6a. The right rectangle shown in Fig. 2a at the absorption time, T = 249.25 min was used.

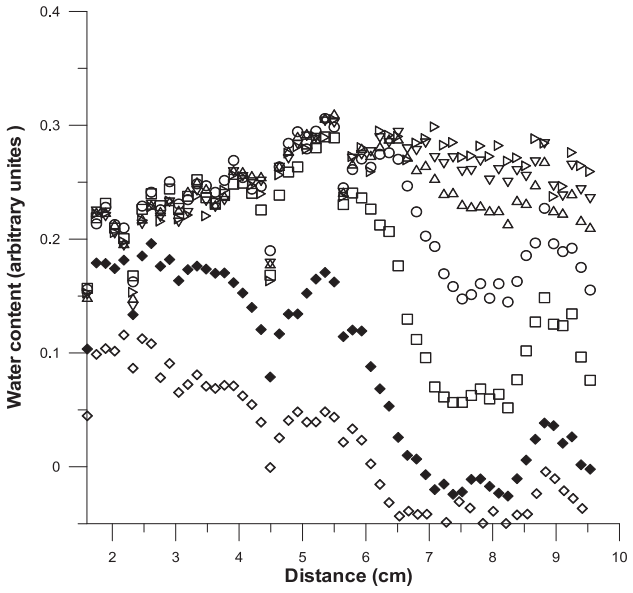

Fig. 7b. Vertical water profiles of the right side of the crack for Mix#2 sample determined at the same absorption times of Fig. 7a.

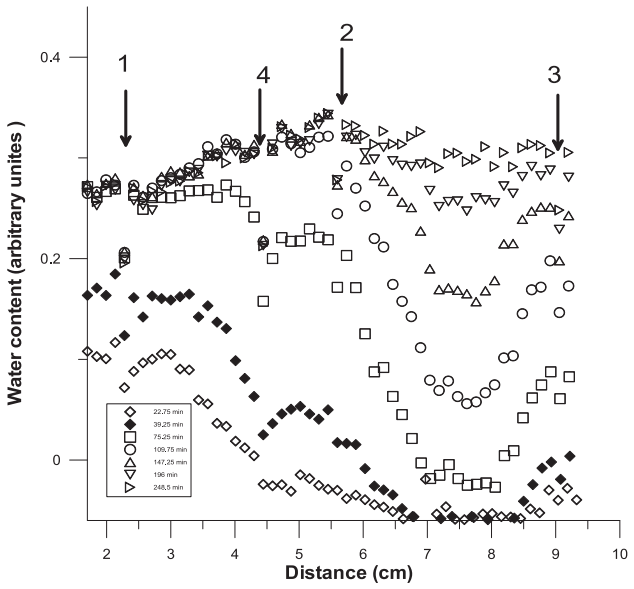

Fig. 7a. Vertical water profiles for the left side of the crack for Mix#2 sample determined at different absorption times. Arrows number 1, 2, and 3 refer to the position of the steel bars. Arrow number 4 refers to a reference line.

3.2. Mix#3 sample

The water absorption into Mix#3 sample was completely different from those of Mix#1 and Mix#2 samples. The external surface of Mix#3 sample was coated with polymeric waterproofing slurry. The NR images (Fig. 8) showed that this sample did not absorb water until an absorption time of ~ 109.75 min. Namely, the external waterproofing agent covering the surface was so effective that it prevented ingress of water into the sample. At the absorption time 109.75 min, it was observed that, the sample started absorbing water only from the crack region dipped in water. The process of water absorption into this sample could be described using the water profiles and progress of the water front through the crack as the absorption time elapses. The rectangular area shown in Fig. 8, at an absorption time 109.75 min, was used to determine the vertical water profiles through the crack. These profiles are shown in Fig. 9a. The profiles represent water distribution through the crack and the surrounded area around it as marked by the rectangle drawn. As one can see, the amount of water absorbed decreases as distance increases in the direction of water flow. From these profiles, the water front position were determined as a function of the square root of the absorption time ($\sqrt{t}$) [71,72] and shown in Fig. 9b. The behavior of the advance of the water front versus $\sqrt{t}$ can be explained as follows: water fills the crack very quickly after an absorption time of 109.75 min (water is sucked by the crack). This is shown in Fig. 9b by the sudden jump of the water front, due to the strong capillary forces, till certain distance along direction of flow (this is marked by the letter S1 in Fig. 9b). Once, the crack is filled it drains water to matrix of the sample (this is marked by the letter D1 in Fig. 9b). One can notice during draining (D1) that, the water front does not advance through the crack. A second sucking – draining (S-D) process and/or cycle is repeated. During this cycle, S2-D2, the crack sucks some water to compensate the water drained (D1). It is characterized with a second sudden rise of the water front through the crack (S2). The sudden rise, S2 is followed by the draining stage (D2 and D3) the process of water absorption into the crack is ended by the third sucking – draining (S3-D3) cycle. The sucking- draining cycles describing the mechanism of water absorption into the crack indicate that the capillary forces causing water suction is hampered and/or resisted by the waterproofing coating, especially during D stages in the S-D cycles. Such kind of competition between the capillary forces and waterproofing coating may depend on the crack geometry (width). A combination of wide cracks (small capillary forces) and the waterproofing coating may succeed in preventing water ingress through the cracks. Thus, the external polymeric waterproofing slurry covering the surface of the sample is effective to protect all regions of the sample against water ingress, except the crack region. It is the weakest region from which water invades the sample.

Once water reached end of the crack (top of the sample) for the Mix#3 sample, it started advancing between the top surface of the sample and the external polymeric waterproofing slurry coating.

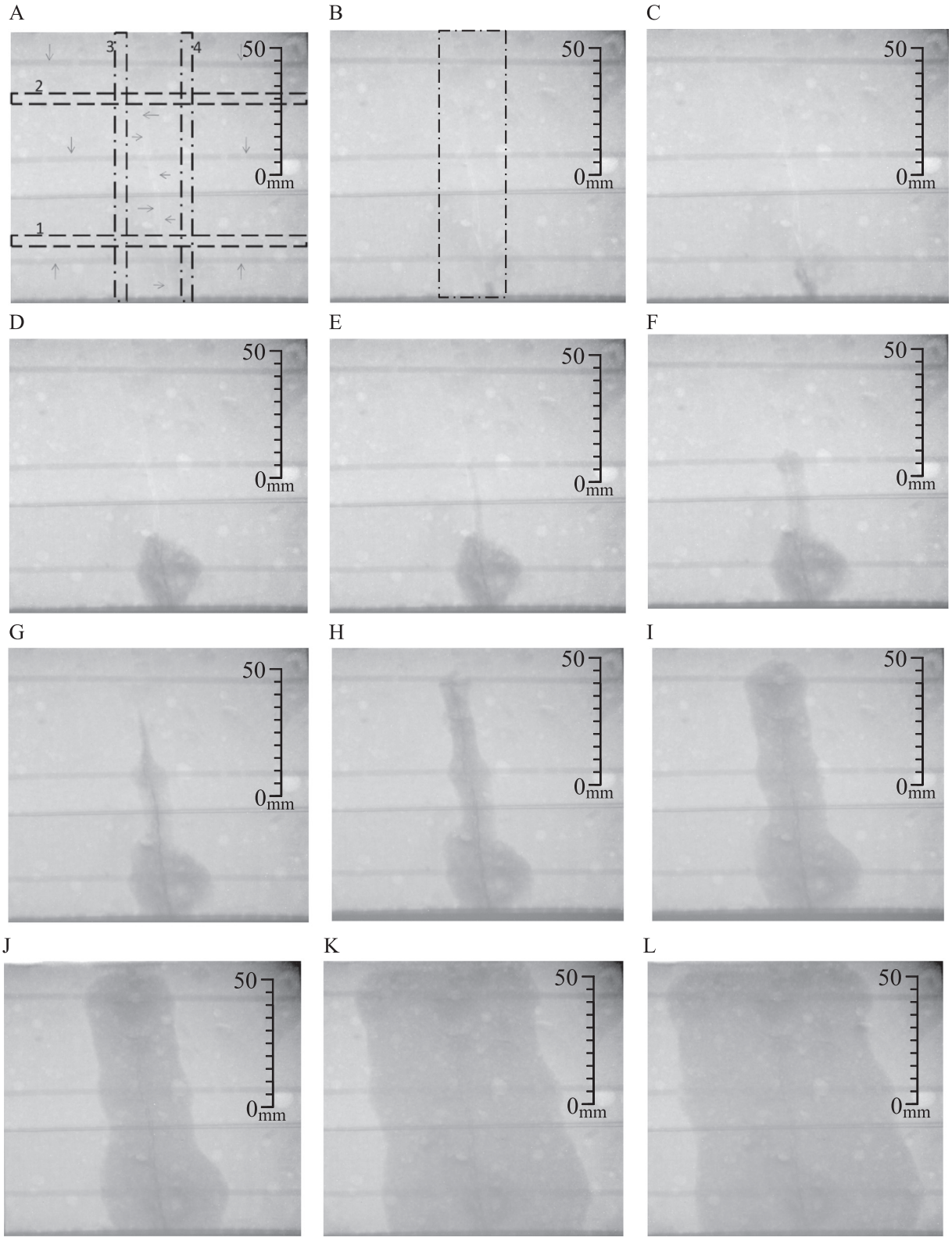

Fig. 8. NR images for Mix# 2 sample recorded at the absorption times 106 min (A), 109.75 min (B), 110.5 min (C), 118.75 min (D), 119.5 min (E), 124.75 min (F), 125.5 min (G), 129.5 min (H), 142 min (I), 168.25 min (J), 322 min (K) and 355.75 min (L) . Image A: the horizontal rectangular areas 1 and 2 refer to two positions at which the horizontal water profiles were determined at both sides of the crack. The vertical rectangular areas 3 and 4 refer to two positions at which the vertical water profiles were determined at both sides of the crack. Image B: the vertical rectangle drawn around the crack refers to the area through which water profiles were determined. The horizontal arrows in image A refer to the crack and the vertical arrows refer to the steel bars.

The progress of such process as the absorption time elapses is shown in Fig. 10. These images were obtained by dividing every image with respect to an image for the dry sample. As one can see, water did not penetrate from upper surface into matrix (down-

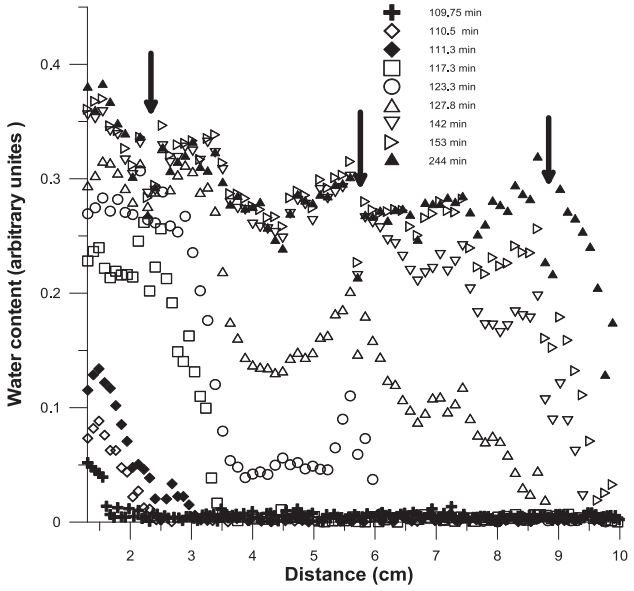

Fig. 9a. Vertical water profiles through the crack for Mix#3 sample at different absorption times. Arrows refer to steel bars positions.

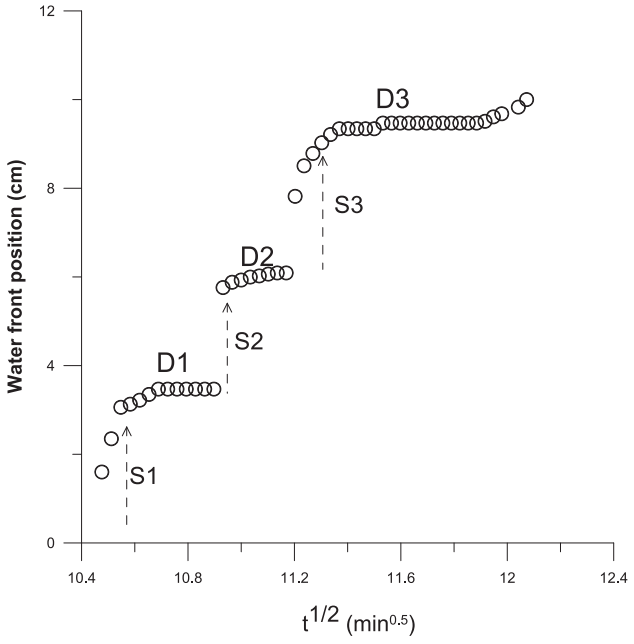

Fig. 9b. Water front position versus square root of absorption time through the crack for Mix#3 sample. The arrows refer to sudden jump of water through the crack (see text for S-D cycles).

ward) of the sample. It means that the polymeric waterproofing slurry coating used protected the sample and prevented water absorption. The coat is not only formed a jacked around surface of the sample, but also it formed a thin film and/or reacted with the surface of the sample. To confirm the present results, further studies should be carried out to investigate the effect of painting different surfaces with the polymeric external waterproofing slurry coating on water absorption. Four different kinds of brick samples were prepared, and all surfaces of them were painted with the polymeric waterproofing slurry. The dimensions of these samples (thickness × width × length) are: 2 × 3.3 × 9 cm, 2 × 3.3 x9.5 cm, 1.65 × 3 × 9.5 cm, and 2.4 × 2.4 × 10 cm, respectively. The outer layers of the polymeric waterproofing slurry were removed from the top and bottom sides of the samples (characterized with small cross section areas). The samples were fixed vertically and their bottom ends were immersed in a water container. Water absorption into these samples was carried out using NR. It was confirmed for one sample that, besides forming a jacked of the coat around the sample, a thin film of the coat was formed on its surface. Water climbed very quickly between the surface covered with thin film and the outer jacket. Further details will be reported and discussed in a forthcoming paper.

It can be noticed, that there are black regions at the top and bottom of the sample around the crack. Additionally, small and large white spots (air bubbles) are distributed through the whole sample. Water preferred spreading around the steel bars as shown in Fig. 10. Rate of steel corrosion could be accelerated, since water may carry dissolved harmful chemicals.

The horizontal spread of water at both sides of the crack was determined at the bottom and top of the Mix#3 sample using the rectangles number 1 and 2 drawn in Fig. 8, at the absorption time 106 min. Figs. 11a and 12a show the profiles at the bottom and top of the sample, respectively. The corresponding water front positions in terms of the absorption time (since water invaded the crack) at the bottom and top of the sample are shown in Figs. 11b and 12b, respectively. The water front positions followed the $\sqrt{t}$ of water absorption at the top and bottom of the samples. The results of Mix#1, Mix#2 and Mix#3 samples were fitted with straight line equation:

$$X = a.\sqrt{t} + b, \quad (1)$$

where X is the water front position, and a and b are fit parameters. The slope a, capillary absorption coefficient, is used to characterize the samples investigated [25,71]. The values of the capillary absorption coefficient are listed in Table 2. Equation (1) is supported by capillary flow theory. It is known as the Washburn equation [73]. As one can see, for Mix#3 sample, water advances faster in the left side direction of the crack, at the top of the sample, than that at the bottom. Whereas, the reverse is true for the advance of water to the right side direction of the crack. The average value of the parameter a for Mix#3 sample (0.195 cm.min$^{-0.5}$), is less than that of Mix#1 and agree with that of Mix#2. It means that water proceeds in the Mix#3 sample slower than that in Mix#1 (79%) and with the same rate as Mix#2 sample. The capillary absorption coefficient values determined in this work (range from 0.18 cm.min$^{-0.5}$ to 0.247 cm.min$^{-0.5}$) are approximately smaller than those reported for water absorption into concrete matrix from a crack of ~ 1.2 cm.min$^{-0.5}$ [73]. Whereas, the values of the capillary absorption coefficient in the present work are more than some values reported for water absorption into mortar, 0.125 cm.min$^{-0.5}$, and concrete, 0.1138 cm.min$^{-0.5}$ [74], ethylene glycol absorption into concrete matrix, 0.0214 cm.min$^{-0.5}$ [75], water absorption into strain hardening cement-based composites, 0.114 cm.min$^{-0.5}$ [57], and concretes (0.089 cm.min$^{-0.5}$ – 0.143 cm.min$^{-0.5}$) [58].

Two vertical rectangular areas (3 and 4), at the left and right sides of the crack and shown in Fig. 8 (at an absorption time T = 106 min) for the Mix#3 sample, were used to determine vertical water profiles. The results are shown in Figs. 13a and 13b, respectively. As one can see, water content is higher at the top of the sample than that at the bottom at both sides of the crack. The profiles for the right side are different from the ones of the left side. The right profiles imply that this side of the sample absorbs more water than the left one. Water contents at top and bottom of the sample are higher than those in the middle of the samples. This can be attributed to the black regions observed at the top and bottom of the sample which accumulates larger quantities of water. These regions were observed in Mix#1 sample. The net

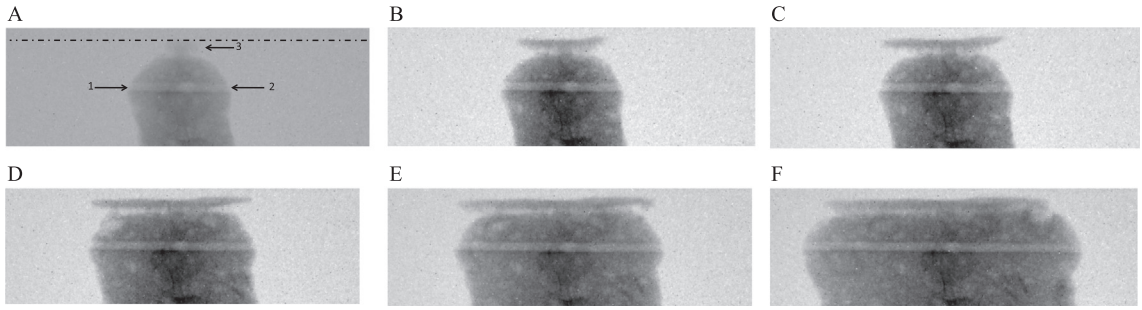

Fig. 10. NR images for the magnified top of Mix#3 sample at the absorption times 145.75 min (A), 160.75 min (B), 169 min (C), 206.5 min (D), 244.75 min (E), and 355.75 min (F). Arrows 1 and 2 refer to the steel bar. Arrow 3 refers to progress of the water layer between upper surface of the sample and the external polymeric waterproofing slurry coating. The dashed line defines the upper surface of the coat.

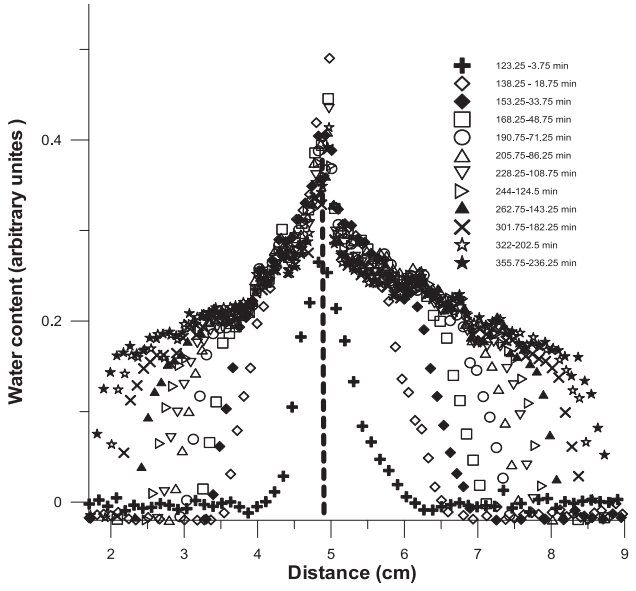

Fig. 11a. Water profiles at both sides of the crack (left and right sides of the crack) for Mix#3 sample at different absorption times (lower position). The first time shown in the legend is the absorption time since the beginning of the experiment and the second time was calculated from the moment water entered the crack region.

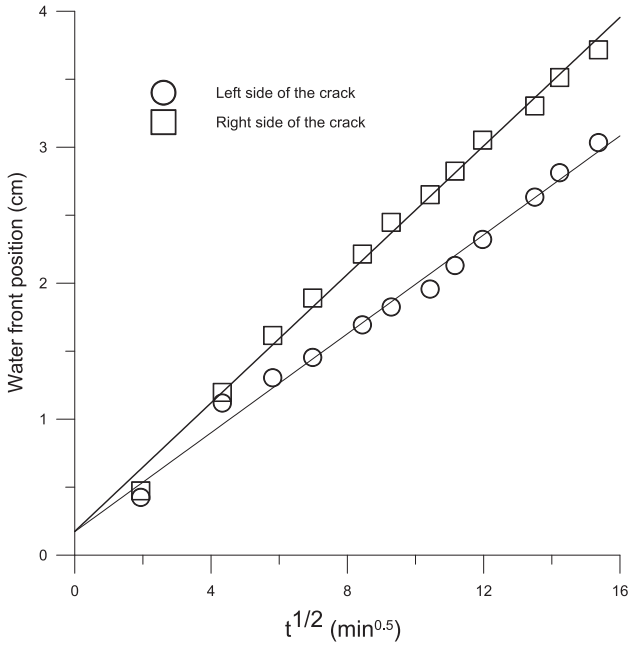

Fig. 11b. Water front position at the left and right sides of the crack versus square root of absorption time for Mix#3 sample extracted from Fig. 11a. The absorption time was calculated from the moment water entered the crack region.

water distribution through Mix#3 was obtained by normalizing a NR image for the sample containing water with respect to an image for the dry sample. The results are shown in Fig. 14. As one can see, the dark area (marked by arrows), are concentrated around the steel bars. They are larger at top than bottom of the sample. These dark regions may be due to unreacted fly ash particles [70]. Additionally, the process of crack induce using a universal testing machine may induce very small cracks, which are not seen in the NR images. These small cracks accumulate water during water absorption.

The waterproof agents used by Duan et al., [41] and/or Xuemet al., [42] altogether with crack sealant agents [43,44] are the best candidates to suppress water ingress in geopolymer materials investigated in this work. This will be reported in a future work.

Neutron radiography was proved to be a powerful non-destructive method for studying moisture transport processes in construction building materials. The method was applied and used successfully for investigating water absorption into bricks and cement-based materials [27,47]. NR was used to study many issues of cracked cement-based materials such as moisture transport, self-healing and internal curing [47]. Other NR studies were carried out for durability issues of concretes including water repellent, delayed ettringite formation, steel reinforced, homogeneity and frost-damaged [47]. However, and to the best knowledge for authors, NR was not used before for studying transport processes in geopolymer samples. Generally, the composition of geopolymer based composites including the samples investigated in this work is completely different from those of cement-based materials and bricks. The present work provides the first successful results on the application of NR method for studying the effect of some hydrophobic treatment methods on water absorption inside cracked geopolymer mortars. The NR images obtained clearly showed the water absorption process inside the cracked geopolymer mortar samples. Cracks are filled quickly with water, then it is distributed to matrix of the samples. Absorbed water carrying harmful chemicals invades regions surrounding the steel bars embedded in the samples investigated. This leads to the possible acceleration of corrosion processes and shorten life cycle of the samples investigated. So, it is urgently needed to find the proper methods to prevent or at least to minimize water absorption insides these samples. Additionally, the present results provide the experimental evidence of that geopolymer mortar samples

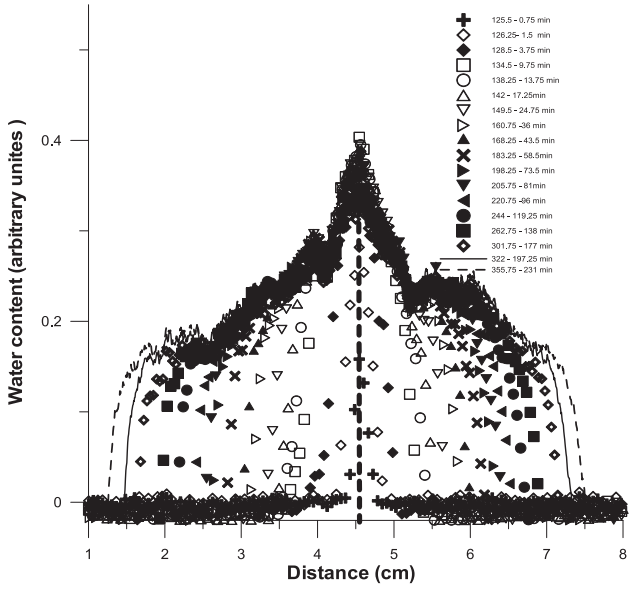

Fig. 12a. Water profiles at both sides of the crack (left and right sides of the crack) for Mix#3 sample at different absorption times for the higher position. The first time shown in the legend is the absorption time since the beginning of the experiment and the second time was calculated from the moment water entered the crack.

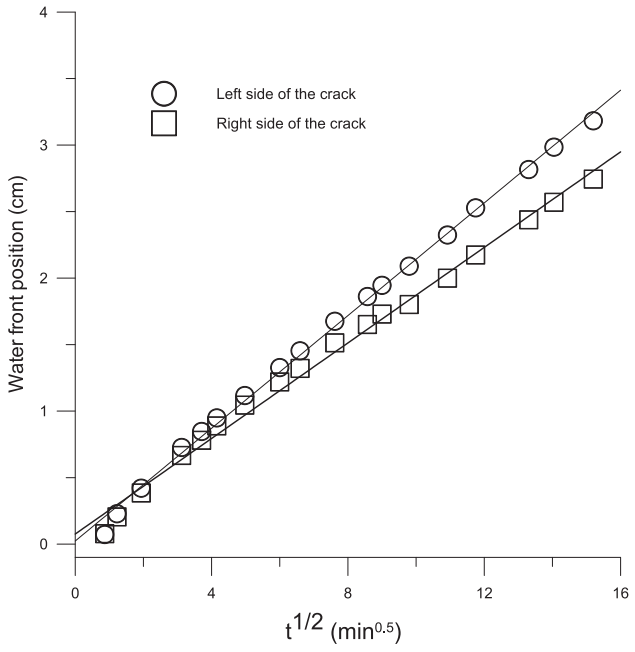

Fig. 12b. Water front position at the left and right sides of the crack versus square root of absorption time for Mix#3 sample extracted from Fig. 12a. The absorption time was calculated from the moment water entered the crack.

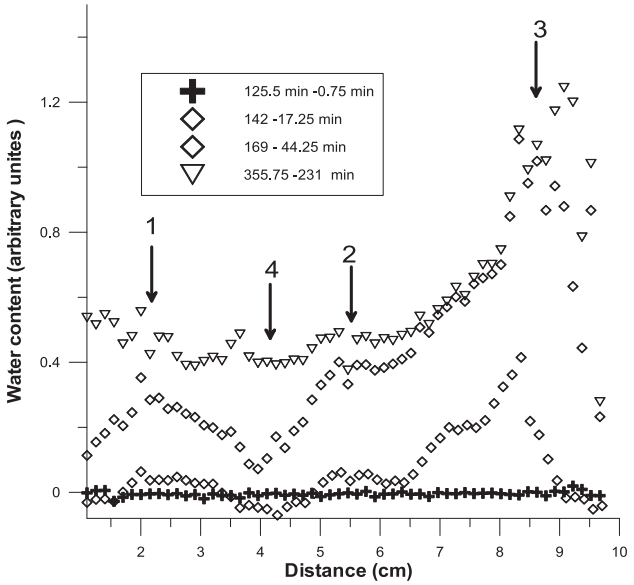

Fig. 13a. Vertical water profiles of the left side of the crack for Mix#3 sample determined at different absorption times.

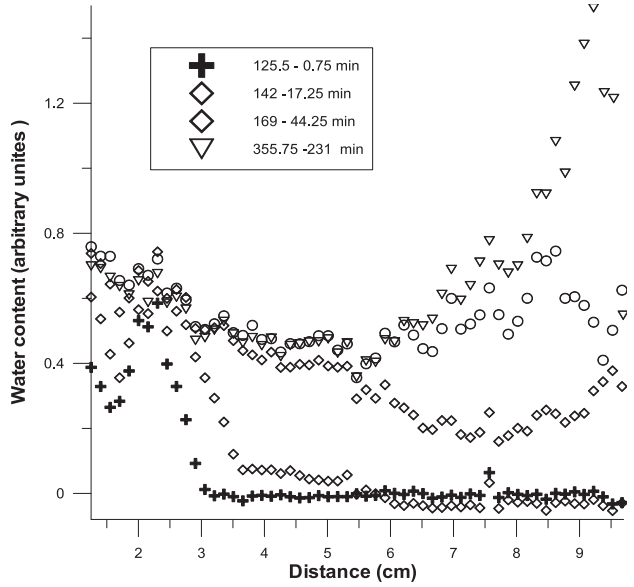

Fig. 13b. Vertical water profiles of the right side of the crack for Mix#3 sample determined at different absorption times.

are transparent for neutrons. Thus, the present work could encourage and accelerate further research work on the use of NR for investigating durability issues of geopolymer based materials. Since the geopolymer mortar samples investigated in this work were prepared under the same curing conditions and mix proportions, their microstructures were kept constant. Thus, the knowledge of the microstructure of the investigated samples is not needed and beyond the scope of the present work.

Table 2
The values of the capillary absorption coefficient at top and bottom (top–bottom) of the investigated samples.

Mix	Mix#1		Mix#2		Mix #3	
a (cm. min$^{-0.5}$)	Left side (top)	Right side (top)	Left side (top)	Right side (top)	Left side (top - bottom)	Right side (top - bottom)
	0.247	x	x	0.194	0.21–0.18	0.174–0.236

[x]the capillary absorption coefficient was not determined at these positions.

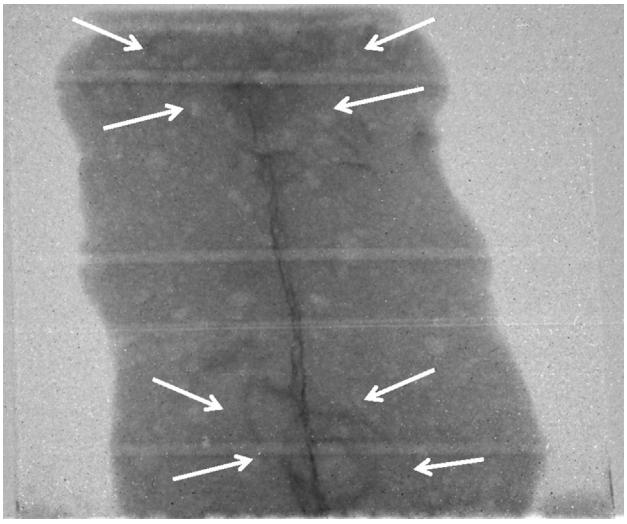

Fig. 14. Net water distribution for Mix#3 sample.

4. Conclusions

Water absorption into cracked geopolymer mortars was investigated for the first time by NR. The results showed that crack of the untreated Mix#1 sample and the sample treated with internal waterproofing additives Mix#2 were filled with water quickly. The internal waterproofing additives used in the Mix#2 sample minimized water absorption. The external polymeric waterproofing slurry coating used in the Mix#3 sample, delayed the water absorption process in comparison with the other samples. It protected all the surface of the sample immersed in water against water absorption except the crack region. It formed a jacket covering the external surface of the sample. It may react with the sample surface forming a film preventing water ingress. Water invaded the Mix#3 sample from the crack region. Mechanism of water filling the crack of Mix#3 sample is different from that of Mix#2 and Mix#1. The matrix of the samples at both sides of the crack was fed with water from filled cracks. Horizontal spread of water through matrix of the samples at both sides of the cracks followed the square root of absorption time. Dark areas were observed in the wetted Mix#1 and Mix#3 samples. These areas could be unreacted fly ash particles or small cracks. White spots were observed through the samples investigated. These spots could be isolated air bubbles. The aluminum adhesive tape used to allow water absorption in one direction should be avoided in forthcoming studies. To increase the resistance of the geopolymer mortars against water absorption, other kinds of agents are needed. Some waterproof and crack sealant agents can be used to suppress water ingress in geopolymer materials.

CRediT authorship contribution statement

A. El Abd: Conceptualization, Methodology, Formal analysis, Writing - original draft, Writing - review & editing, Supervision, Investigation. **S.E. Kichanov:** Methodology, Software, Data curation, Resources. **M. Taman:** Conceptualization, Methodology, Formal analysis, Visualization, Investigation, Resources, Data curation, Writing - original draft, Writing - review & editing. **K. M. Nazarov:** Software, Investigation, Data curation, Resources.

Declaration of Competing Interest

The authors declare that they have no known competing financial interests or personal relationships that could have appeared to influence the work reported in this paper.

Acknowledgement

The academy of scientific research and technology of Egypt (ASTR) is gratefully acknowledged for their financial support for this work. The results presented in this article rely on 3rd phase of collaboration projects between ASTR and Joint Institute for Nuclear Research (JINR), Dubna, Russia.

References

[1] Scrivener KL, Kirkpatrick RJ. Innovation in use and research on cementitious material. In: 12th International congress of chemistry of cement, Montreal, Canada; 2007.
[2] Malhotra VM, Mehta PK. High-performance, high-volume fly ash concrete: materials, mixture, proportioning, properties, construction practice, and case histories. 2nd Supplementary cementing materials for sustainable development incorporated, Ottawa; 2005. p. 1–124.
[3] G.L. Golewski, Green concrete composite incorporating fly ash with high strength and fracture toughness, J. Cleaner Prod. 172 (2018) 218–226.
[4] H.F.W. Taylor, Cement chemistry, Thomas Telford, London, 1997.
[5] M. Malhotra, Introduction: Sustainable Development and Concrete technology, ACI Concr. J. (2000) 1147–1165.
[6] P.K. Mehta, Reducing the Environmental Impact of Concrete, Concr. Int. (2001) 61–66.
[7] A.K. Saha, Effect of class F fly ash on the durability properties of concrete, Sustainable Environ. Res. 28 (1) (2018) 25–31.
[8] R. Siddique, Performance characteristics of high-volume Class F fly ash concrete, Cem. Concr. Res. 34 (3) (2004) 487–493.
[9] A.K. Saha, P.K. Sarker, Sustainable use of ferronickel slag fine aggregate and fly ash in structural concrete: Mechanical properties and leaching study, J. Cleaner Prod. 162 (2017) 438–448.
[10] D. Shen, C. Liu, Z. Feng, S. Zhu, C. Liang, Influence of ground granulated blast furnace slag on the early-age anti-cracking property of internally cured concrete, Constr. Build. Mater. 223 (2019) 233–243.
[11] Y. Zhao, J. Gong, S. Zhao, Experimental study on shrinkage of HPC containing fly ash and ground granulated blast-furnace slag, Constr. Build. Mater. 155 (2017) 145–153.
[12] D. Shen, K. Liu, C. Wen, Y. Shen, G. Jiang, Early-age cracking resistance of ground granulated blast furnace slag concrete, Constr. Build. Mater. 222 (2019) 278–287.
[13] Chi, M.C., Chi, J.H. and Wu, C.H., 2018. Effect of GGBFS on compressive strength and durability of concrete. In Advanced Materials Research (Vol. 1145, pp. 22-26). Trans Tech Publications.
[14] D. Shen, Y. Jiao, J. Kang, Z. Feng, Y. Shen, Influence of ground granulated blast furnace slag on early-age cracking potential of internally cured high performance concrete, Constr. Build. Mater. 233 (2020) 117083.
[15] J. Ren, L. Zhang, R. San Nicolas, Degradation process of alkali-activated slag/fly ash and Portland cement-based pastes exposed to phosphoric acid, Constr. Build. Mater. 232 (2020) 117209.
[16] F. Nosouhian, M. Fincan, N. Shanahan, Y.P. Stetsko, K.A. Riding, A. Zayed, Effects of slag characteristics on sulfate durability of Portland cement-slag blended systems, Constr. Build. Mater. 229 (2019) 116882.
[17] R.K. Majhi, A.N. Nayak, Bond, durability and microstructural characteristics of ground granulated blast furnace slag based recycled aggregate concrete, Constr. Build. Mater. 212 (2019) 578–595.
[18] J. Davidovits, Geopolymers: inorganic polymeric new materials, J. Therm. Anal. 37 (1991) 1633–1656.
[19] Davidovits J. Mineral polymers and methods of making them. US patent no. 4349, 386; 1982.
[20] D. Hardjito, S.E. Wallah, D.M.J. Sumajouw, B.V. Rangan, On the development of fly ash-based geopolymer concrete, ACI Mater. J. 101 (2004) 467–472.
[21] J. Wongpa, K. Kiattikomoi, C. Jaturapitakkul, P. Chindaprasirt, Compressive strength, modulus of elasticity, and water permeability of inorganic polymer concrete, Mater. Des. 31 (2010) 4748–4754.
[22] G. Kovalchuk, A. Fernandez-Jimenez, A. Palomo, Alkali-activated fly ash: effect of thermal curing conditions on mechanical and microstructural development-Part II, Fuel 86 (2007) 315–322.
[23] Z. Huajun, Z. Zuhua, Z. Yingcan, T. Liang, Durability of alkali-activated fly ash concrete: Chloride penetration in pastes and mortars, Constr. Build. Mater. 65 (2014) 51–59.
[24] A. Hoła, Ł. Sadowski, A method of the neural identification of the moisture content in brick walls of historic buildings on the basis of non-destructive tests, Autom. Constr. 106 (2019) 102850.
[25] M.S. Camino, F.J. León, A. Llorente, J.M. Olivar, Evaluation of the behavior of brick tile masonry and mortar due to capillary rise of moisture, Materiales de Construcción 64 (314) (2014) 020.
[26] A. Leemann, B. Lothenbach, C. Hoffmann, Biologically induced concrete deterioration in a wastewater treatment plant assessed by combining microstructural analysis with thermodynamic modeling, Cem. Concr. Res. 40 (2010) 1157–1164.
[27] P. Zhang, F.H. Wittmann, P. Lura, H.S. Müller, S. Han, T. Zhao, Application of neutron imaging to investigate fundamental aspects of durability of cement-based materials: A review, Cem. Concr. Res. 108 (2018) 152–166.

[28] F.C. De Beer, W.J. Strydom, E.J. Griesel, The drying process of concrete: a neutron radiography study, Appl. Radiat. Isot. 61 (2004) 617–623.
[29] B. Villmann, V. Slowik, F.H. Wittmann, P. Vontobel, J. Hovind, Time-dependent moisture distribution in drying cement mortars - results of neutron radiography and inverse analysis of drying tests, Restor. Build. Monum. 20 (2014) 49–62.
[30] P. Zhang, F.H. Wittmann, M. Haist, H.S. Müller, P. Vontobel, T.J. Zhao, Water penetration into micro-cracks in reinforced concrete, Restor. Build. Monum. 20 (2014) 85–94.
[31] P. Zhang, F.H. Wittmann, T. Zhao, E.H. Lehmann, Neutron imaging of water penetration into cracked steel reinforced concrete, Phys. B 405 (2010) 1866–1871.
[32] Z.F. Yang, W.J. Weiss, J. Olek, Water transport in concrete damaged by tensile loading and freeze-thaw cycling, J. Mater. Civ. Eng. 18 (2006) 424–434.
[33] P. Zhang, F.H. Wittmann, M. Vogel, H.S. Müller, T.J. Zhao, Influence of freeze thaw cycles on capillary absorption and chloride penetration into concrete, Cem. Concr. Res. 100 (2017) 60–67.
[34] F. Liu, Z. You, X. Yang, H. Wang, Macro-micro degradation process of fly ash concrete under alternation of freeze-thaw cycles subjected to sulfate and carbonation, Constr. Build. Mater. 181 (2018) (2018) 369–380.
[35] V. Picandet, A. Khelidj, H. Bellegou, Crack effects on gas and water permeability of concretes, Cem. Concr. Res. 39 (2009) 537–547.
[36] H.S. Müller, M. Haist, M. Vogel, Assessment of the sustainability potential of concrete and concrete structures considering their environmental impact, performance and lifetime, Constr. Build. Mater. 67 (2014) 321–337.
[37] U.M. Angst, R.D. Hooton, J. Marchand, C.L. Page, R.J. Flatt, B. Elsener, C. Gehlen, J. Gulikers, Present and future durability challenges for reinforced concrete structures, Mater. Corros. 63 (2012) 1047–1051.
[38] T. Nemec, J. Rant, V. Apih, B. Glumac, Study of building materials impregnation processes by quasi-real-time neutron radiography, Nucl. Instr. Meth. Phys. Res. A 424 (1999) 242–247.
[39] S.R. White, N.R. Sottos, J. Moore, P. Geubelle, M. Kessler, E. Brown, S. Suresh, S. Viswanathan, Autonomic healing of polymer composites, Nature 409 (2001) 794–797.
[40] J. Zhang, C. Shi, Z. Zhang, Z. Ou, Durability of alkali-activated materials in aggressive environments: A review on recent studies, Constr. Build. Mater. 152 (2017) 598–613.
[41] P. Duan, C. Yan, W. Luo, W. Zhou, A novel surface waterproof geopolymer derived from metakaolin by hydrophobic modification, Mater. Lett. 164 (2016) 172–175.
[42] X. Xue Y.-L. Liu J.-G. Dai Poon C-Sn, Zhang W-D, Zhang P., Inhibiting efflorescence formation on fly ash–based geopolymer via silane surface modification Cement and Concrete Composites 94 2018 43 52
[43] K. Van Tittelboom, N. De Belie, D. Van Loo, P. Jacobs, Self-healing efficiency of cementitious materials containing tubular capsules filled with healing agent, Cem. Concr. Compos. 33 (2011) 497–505.
[44] K. Van Tittelboom, D. Snoeck, P. Vontobel, F. Wittmann, De Belie Nele, Use of neutron radiography and tomography to visualize the autonomous crack sealing efficiency in cementitious materials, Mater. Struct. 46 (2013) 105–121.
[45] J.C. Domanus (Ed.), Practical Neutron Radiography, Kluwer Academic Publisher, Dordrecht, 1992.
[46] A. Harms, D. Wyman, Mathematics and Physics of Neutron Radiography, Kluwer Academic Publisher, Dordrecht, 1986.
[47] E. Perfect, C.-L. Cheng, M. Kang, H.Z. Bilheux, J.M. Lamanna, M.J. Gragg, D.M. Wright, Neutron imaging of hydrogen-rich fluids in geomaterials and engineered porous media: A review, Earth Sci. Rev. 129 (2014) 120–135.
[48] M. Strobl, I. Manke, N. Kardjilov, A. Hilger, M. Dawson, J. Banhart, Advances in neutron radiography and tomography, J. Phys. D. Appl. Phys. 42 (2009) 43001–43021.
[49] N. Kardjilov, I. Manke, A. Hilger, M. Strobl, Neutron imaging in materials science, Mater. Today 14 (2011) 248–256.
[50] F.C. De Beer, Neutron- and X-ray radiography/tomography: non-destructive analytical tools for the characterization of nuclear materials, J. S. Afr. I. Min. Metall. 115 (2015) 913–924.
[51] B. Winkler, Applications of neutron radiography and neutron tomography, Rev. Mineral. Geochem. 63 (2006) 459–471.
[52] A.P. Kaestner, P. Trtik, M. Zarebanadkouki, D. Kazantsev, M. Snehota, K.J. Dobson, E.H. Lehmann, Recent developments in neutron imaging with applications for porous media research, Solid Earth 7 (2016) 1281–1292.
[53] A. El Abd, J.J. Milczarek, Neutron radiography study of water absorption in porous building materials: anomalous diffusion analysis, J. Phys. D 37 (2004) 2305.
[54] A.E. El Abd, A. Czachor, J.J. Milczarek, J. Pogorzelski, Neutron radiography studies of water migration in construction porous materials, IEEE Trans. Nucl. Sci. 52 (2005) 229–304.
[55] A. El Abd, A. Czachor, J. Milczarek, Neutron radiography determination of water diffusivity in fired clay brick, Appl. Radiat. Isot. 47 (2009) 556–559.
[56] N. Alderete, Y.V. Zaccardi, D. Snoeck, B. Van Belleghem, P. Van den Heede, K. Van Tittelboom, N. De Belie, Capillary imbibition in mortars with natural pozzolan, limestone powder and slag evaluated through neutron radiography, electrical conductivity, and gravimetric analysis, Cem. Concr. Res. 118 (2019) 57–68.
[57] P. Zhang, F.H. Wittmann, T.J. Zhao, E.H. Lehmann, L. Tian, P. Vontobel, Observation and quantification of water penetration into Strain Hardening Cement-based Composites (SHCC) with multiple cracks by means of neutron radiography, Nuclear Instruments and Methods in Physics Research A 620 (2010) 414–420.
[58] P. Zhang, F.H. Wittmann, T.J. Zhao, E.H. Lehmann, P. Vontobel, Neutron radiography, a powerful method to determine time-dependent moisture distributions in concrete, Nucl. Eng. Des. 241 (2011) 4758–4766.
[59] P. Zhang, P. Wang, D. Hou, Z. Liu, M. Haist, T. Zhao, Application of neutron radiography in observing and quantifying the time-dependent moisture distributions in multi-cracked cement based composites, Cem. Concr. Compos. 78 (2017) 13–20.
[60] P. Zhang, Z. Liu, S. Han, L. He, H.S. Müller, T. Zhao, Y. Wang, Visualization of rapid penetration of water into cracked cement mortar using neutron radiography, Mater. Lett. (2017), https://doi.org/10.1016/j.matlet.2017.02.077.
[61] C. Schrofl, V. Mechtcherine, A. Kaestner, P. Vontobel, J. Hovind, E. Lehmann, Transport of water through strain-hardening cement-based composite(SHCC) applied on top of cracked reinforced concrete slabs with and without hydrophobization of cracks – Investigation by neutron radiography, Constr. Build. Mater. 76 (2015) 70–86.
[62] P. Van den Heede, B. Van Belleghem, N. Alderete, K. Van Tittelboom, N. De Belie, Neutron Radiography Based Visualization and Profiling of Water Uptake in (Un) cracked and Autonomously Healed Cementitious, Materials, Materials 9 (2016) 311, https://doi.org/10.3390/ma9050311.
[63] D.P. Kozlenko, S.E. Kichanov, E.V. Lukin, A.V. Rutkauskas, G.D. Bokuchava, B.N. Savenko, A.V. Pakhnevich, A.Yu. Rozanov, Neutron Radiography Facility at IBR-2 High Flux Pulsed Reactor: First Results, Physics Procedia 69 (2015) 87–91.
[64] D.P. Kozlenko, S.E. Kichanov, E.V. Lukin, A.V. Rutkauskas, A.V. Belushkin, G.D. Bokuchava, B.N. Savenko, Neutron radiography and tomography facility at IBR-2 reactor, Phys. Part. Nuclei Lett. 13 (2016) 346–351.
[65] C.A. Schneider, W.S. Rasband, K.W. Eliceiri, NIH Image to ImageJ: 25 years of image analysis, Nat. Methods. 9 (2012) 671–675.
[66] I. Topçu, Ö. Atesin, Effect of high dosage lignosulphonate and naphthalene sulphonate based plasticizer usage on micro concrete properties, Constr. Build. Mater. 120 (2016) 189–197.
[67] A.M. Rashad, A comprehensive overview about the influence of different additives on the properties of alkali-activated slag – A guide for Civil Engineer, Constr. Build. Mater. 47 (2013) (2013) 29–55.
[68] A.M. Rashad, A comprehensive overview about the influence of different admixtures and additives on the properties of alkali-activated fly ash, Mater. Des. 53 (2014) 1005–1025.
[69] T. Bakharev, J.G. Sanjayan, Y.-B. Cheng, Effect of admixtures on properties of alkali-activated slag concrete, Cem Concr Res 30 (2000) 1367–1374.
[70] A. Fernandez-Jimenez, A. Palomo, Composition and microstructure of alkali activated fly ash binder: Effect of the activator, Cem. Concr. Res. 35 (10) (2005) 1984–1992.
[71] B.S. Nabawy, C. David, X-ray CT scanning imaging for the Nubia sandstone as a tool for characterizing its capillary properties, Geosci J 20 (2016) 691–704.
[72] C. David, D. Bertauld, J. Dautriat, J. Sarout, B. Menéndez, B. Nabawy, Detection of moving capillary front in porous rocks using X-ray and ultrasonic methods, Front. Phys. 3 (2015) 53.
[73] N. Tsuchiya, M. Kanematsu, T. Noguchi, Quick water movement around concrete cracks under unsaturated conditions, Constr. Build. Mater. 67 (2014) 95–99.
[74] L. Yang, D. Gao, Y. Zhang, J. Tang, Relationship between sorptivity and capillary coefficient for water absorption of cement-based materials: theory analysis and experiment, R. Soc. open sci. 6 (2019) 190112.
[75] L. Hanzić, L. Kosec, I. Anzel, Capillary absorption in concrete and the Lucas-Washburn equation, Cem. Concr. Compos. 32 (2010) 84–91.